Clim Dyn
DOI 10.1007/s00382-008-0490-7

The role of MJO and mid-latitude fronts in the South China Sea summer monsoon onset

H. W. Tong · Johnny C. L. Chan · W. Zhou

Received: 13 May 2008 / Accepted: 3 November 2008

Abstract Previous studies have suggested that the South China Sea (SCS) summer monsoon onset is concurrent with the arrival of a 30–60-day northward-propagating trough. On the other hand, from a synoptic viewpoint, some studies pointed out that the arrival of a mid-latitude front may be the triggering mechanism of the SCSSM onset. This study attempts to link these two viewpoints and to investigate their relative role in inducing the SCSSM onset. Composites of low-level zonal winds, geopotential heights and temperatures during the 1991–1999 SCSSM onsets based on the European Centre for Medium Range Weather Forecast ERA-40 data indicate that both the Madden and Julian Oscillation (MJO)/Kelvin waves and mid-latitude trough are apparently involved in the onset. The MJO/Kelvin waves play a major role in inducing the large-scale easterly-westerly shift over the central SCS, while the effect of the acceleration of westerlies ahead of the mid-latitude trough is limited to the northern SCS only. Numerical experiments using a regional climate model further demonstrate that the MJO/Kelvin waves control the timing of the onset by changing the background meridional geopotential height gradient over the SCS. When the MJO is at its peak phase over the Maritime continent, it imposes a positive meridional geopotential height gradient over the SCS such that easterly winds are induced, which significantly reduces the strength of a mid-latitude trough. After the equatorial convection has dissipated, a Rossby-wave response is induced, leading to the formation of a northward-moving trough. When this trough moves northward, the meridional geopotential height gradient is reversed and westerly winds are induced. At the same time, if a mid-latitude trough arrives in south China, the westerlies associated with the mid-latitude trough will strengthen because of the background meridional geopotential height gradient, which gives the impression that both the northward-moving trough and mid-latitude trough are in phase and work together to induce the onset.

H. W. Tong · J. C. L. Chan (✉) · W. Zhou
Guy Carpenter Asia-Pacific Climate Impact Centre,
City University of Hong Kong, Tat Chee Ave.,
Kowloon, Hong Kong, China
e-mail: Johnny.Chan@cityu.edu.hk

1 Introduction

Early literature (e.g. Tao and Chen 1987) suggested that the East Asian summer monsoon first takes place over the South China Sea (SCS). Although later observations found that the Bay of Bengal (BOB) onset usually precedes the SCS summer monsoon (SCSSM) onset by one pentad (Ding and Liu 2001), the SCSSM onset still receives much attention as it usually marks the beginning of the rainy season over China. Therefore, the timing and the onset process is of particular interest.

Since the discovery of the 30–40-day tropical oscillation [Madden and Julian (1971, 1972); usually referred to as Madden and Julian Oscillation, or MJO], many studies have been devoted to the linkage between this intraseasonal oscillation (ISO) and the various monsoon systems. In the boreal winter, the MJO is basically an eastward-propagating phenomenon with little meridional propagation (Madden 1986; Hendon and Salby 1994). However, in the boreal summer, the MJO displays a more complex behavior. Apart from the eastward propagation, the MJO also propagates poleward over the Indian Ocean and the western North Pacific (WNP), with the northern branch being significantly stronger than the southern branch (Lawrence

Published online: 25 November 2008

and Webster 2002). This northward-propagating ISO may therefore influence the life cycle, active and break periods and even the onset of the various components of the East Asia summer monsoon.

Krishnamurti and Subrahmanyam (1982) found a northward propagation of an ISO over the Indian monsoon region with a time-scale of 30–50 days. They also found that this mode exists from early May to late June and showed that the active (break) period of the monsoon coincides with the arrival of the 30–50-day tough (ridge). Chen and Chen (1995) observed a similar pattern over the SCS. They studied the 1979 SCSSM life cycle and also found northward-propagating troughs (ridges) that controlled the active (break) periods of the monsoon. They suggested that the northward-propagating troughs/ridges are coupled with the eastward-propagating 30–60-day mode of the global divergent circulation. Chan et al. (2002) found that the 1998 SCSSM onset emerged when the 30–60-day northward-propagating trough arrived in the SCS. Wang and Xu (1997) further pointed out that the northward-propagating ISO was coupled with the slow annual cycle such that the climatological ISO was statistically significant. This apparently explains why the SCSSM onset takes place regularly around mid-May every year.

Recently, Straub et al. (2006) suggested that the SCSSM onset, or more specifically, the westerlies onset is closely related to the MJO and Kelvin waves. They used a 25-year composite to show that the onset is triggered by the westerly winds associated with the wake of the MJO or Kelvin wave.

On the other hand, from a synoptic viewpoint, Chang and Chen (1995) and Chan et al. (2000) both pointed out that the arrival of a mid-latitude front may be the triggering mechanism of the SCSSM onset. Chan et al. (2000) suggested that the atmosphere may have become unstable prior to the onset. Monsoon onset occurs only when the convective available potential energy is released by the approach of a mid-latitude front. This could explain the abruptness of the SCSSM onset. However, this raises an important question: what makes the triggering front so special that only this front can trigger the onset? In addition, what is the linkage between the synoptic-scale disturbances and the 30–60-day ISO? The objective of this study is therefore to investigate how these two very different time-scale oscillations might collaborate with each other and their relative roles during the onset period.

The data used are described in Sect. 2 followed by a composite study of the 1991–1999 SCSSM onset in Sect. 3. Numerical experiments are also carried out to ascertain further the findings in the composite study. The model description, experiment setups and results are discussed in Sect. 4. Section 5 gives the conclusion and discussion.

2 Data and onset date

2.1 Data

The following data are used: 6 hourly reanalysis of the European Centre for Medium Range Weather Forecasts ERA-40 data set for 1991–1999, the daily outgoing longwave radiation (OLR) from the US National Centers for Environmental Prediction (NCEP) for the same period. The OLR data are used as a proxy for deep convection. Both datasets have a horizontal resolution of 2.5° latitude × 2.5° longitude.

2.2 Definition of onset date

Following Mao and Chan (2005), the SCSSM onset date for each individual year is defined as the day when the area-average of 850-hPa zonal wind over the SCS (110–120°E, 5–20°N) changes from negative to positive and remains positive for more than 6 days. The onset dates for 1991–1999 are shown in Table 1. Composites of various parameters are then constructed based on the onset date.

3 Composite study

3.1 Brief description of the onset

The SCSSM onset is characterized by its abrupt change of zonal wind direction. This can be clearly seen in the time-latitude plot of the composite 850-hPa zonal winds averaged over the SCS domain (Fig. 1a). Day 0 is the onset date of the composite. Prior to day 0, the SCS is dominated by easterly winds. Easterly winds are then suddenly replaced by westerly winds on day 0. Straub et al. (2006) shows that this kind of large-scale easterly-westerly shift could be associated with the passage of an MJO over the equatorial Indian Ocean and the subsequent emanation of a moist Kelvin wave into the equatorial Pacific (see their

Table 1 Dates of the SCSSM onset during 1991–1999 (month-day)

Year	Onset date
1991	6–08
1992	5–16
1993	6–04
1994	5–02
1995	5–12
1996	5–06
1997	5–16
1998	5–20
1999	4–22

Fig. 3). The time-latitude cross-section of OLR shows that the onset is indeed closely related to the eastward propagation of convection along the equator (marked by a solid arrow in Fig. 1b). Apart from this large-scale change, an equatorial propagation of westerly winds just before the onset (marked by a solid arrow in Fig. 1a) can also be seen. These westerly winds are in fact associated with the southern frank of an equatorward-moving mid-latitude trough as suggested by the time-latitude cross-section of 850-hPa geopotential height (Fig. 1c). Behind this trough is usually a pool of cold air from the mid-latitudes. The cold air reaches the northern SCS with a time-lag of 2–3 days (Fig. 1d). This is consistent with Chang and Chen (1995) and Chan et al. (2000) that the SCSSM onset involves the intrusion of a mid-latitude front. Chan et al. (2000) argued that this equatorward-moving mid-latitude front could realize the convective available potential energy and trigger the deep convection over the SCS.

This composite shows that both the passage of MJO and the intrusion of mid-latitude front are common during the SCSSM onset. These two phenomena are very different in both the spatial and temporal timescales. In order to separate these two modes, a first-order Butterworth bandpass filter is applied to the composite. Two ranges of bandpass filtering are used to isolate the intraseasonal mode (30–60 days) and synoptic-scale mode (5–20 days). The 5–20-day filtering is intended instead of the usual 10–20-day filtering because we want to include mid-latitude systems that usually have a higher frequency than those northwestward-propagating disturbances over the WNP (Chan et al. 2002). Their relative roles on the SCSSM onset will be discussed in more detail in the next section.

3.2 The 30–60-day mode

The evolution of the 30–60-day mode 850-hPa height anomalies shows that in pentad −2 (two pentads before the onset), a low height anomaly is crossing the Indian Ocean (Fig. 2a). The shape of this anomaly has some resemblance with the Gill's response to a heat source over the tropics.

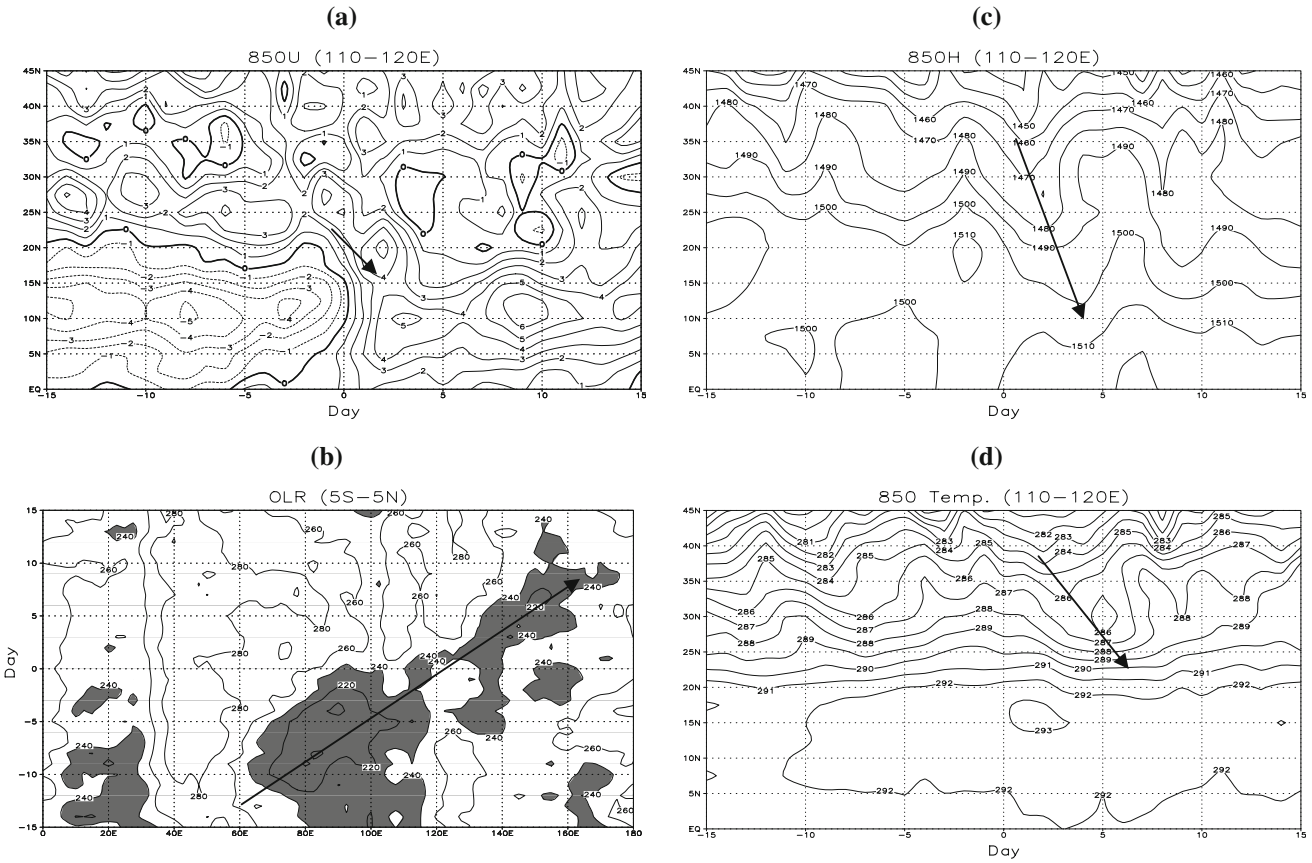

Fig. 1 **a** Time-latitude cross-section of composite 850-hPa zonal wind (m s^{-1}) averaged over 110–120°E. *Solid arrow* represents the equatorial propagation of westerlies. **b** Time-longitude cross-section of composite of composite OLR averaged over 5°S–5°N. Values $\leq$ 240 W m^{-2} are *shaded*. *Solid arrow* represents the eastward propagation of convection. **c** Same as **a**, but for 850-hPa geopotential height (gpm). *Solid arrow* represents the equatorward propagation of geopotential height. **d** Same as **a**, but for 850-hPa temperature (K). *Solid arrow* represents the equatorward propagation of temperature. Day 0 is the onset day and negative (positive) days indicate the number of days prior to (after) the onset

Notice also the twin vortices straddling the equator in the Indian Ocean. Easterly winds are ahead of the convective centre (see also Fig. 1b) with strong westerlies at the wake, which strongly suggests that this feature is an MJO. A low anomaly also develops over central China, which does not appear to be directly linked to the MJO. The low anomaly over China strengthens slightly and moves to the coast of south China by pentad −1 (Fig. 2b). Westerly winds are induced in the southern flank of this low anomaly. These westerly winds together with the easterly winds induced ahead of the MJO centre act to enhance the anticyclone over the SCS. During the onset pentad (pentad 0), the southern cyclone dissipates over the southern Indian Ocean while the northern one moves northwestward and reaches the eastern coast of India (Fig. 2c). The low anomaly over China now splits into two centres, one over south China, and one to the southeast of Japan. Previous studies have suggested that the cyclone over the BOB could induce an asymmetric Rossby wave response, which is similar to the low anomaly over south China (Liu et al. 2002). Therefore, whether the low anomaly originates purely from the mid-latitudes or partly contributed by the BOB cyclone needs further investigation, but is beyond the scope of the current study. Strong westerly winds now extend from BOB and Indochina to the SCS, which marks the onset of the SCSSM. By pentad +1, the westerly winds extend all the way to 150°E and a cyclonic shear zone is formed over the northern SCS (not shown).

To examine how much the 30–60-day mode plays in inducing the onset, the explained variance of the 850-hPa zonal wind anomalies by the 30–60 filtered 850-hPa zonal wind for day −15 (the 15th day before onset) to day +15 (the 15th day after the onset) at every grid point is calculated. The period is chosen because it is about half a cycle of the 30–60-day mode and this ensures that both the 30–60-day mode and 5–20-day mode variability can be captured. Areas of explained variance exceeding 90% are clearly seen over the equatorial Indian Ocean and are associated with the MJO (Fig. 3). Areas of explained variance exceeding 80% can be also seen over the central SCS and southeast of the Philippines. This result suggests that the MJO and its associated large-scale easterly-westerly shift play a major role in inducing the SCSSM onset, especially the central SCS.

3.3 The 5–20-day mode

The evolution of the 5–20-day mode composite 850-hPa height and wind fields shows a ridge dominating over the SCS, the East China Sea and the south of Japan on day −2 (Fig. 4a). Easterly winds are dominating over the SCS. Southwesterly winds can also be seen in the southwestern frank of the ridge at around 110–120°E, 27–33°N. On day −1, the ridge is still covering the SCS with easterly winds still dominating (Fig. 4b). The westerlies over central China strengthen and move southward due to the developing low anomaly over the northwestern part of China. On day 0, the ridge weakens significantly (Fig. 4c). The low anomaly also deepens into a closed low and strong southwesterly winds are now located at 110–120°E, 25–30°N. This equatorward movement of westerly winds is clearly depicted in Fig. 1a. Although the ridge has weakened significantly, it is interesting to note that the general wind direction over the SCS is still easterly. This indicates clearly that the abrupt shift of wind direction from easterly to westerly on day 0 in the composite can hardly be attributed to the 5–20-day mode. By day +2, the closed low has moved to south China and formed a trough-like feature covering the northern SCS and part of the WNP (Fig. 4d). It appears that another mid-latitude cyclone is developing over the Yellow Sea centered at 120°E, 37°N. On day +3, the mid-latitude cyclone deepens and moved eastward, joining the trough that originally covered the northern SCS to form an extensive region of low-height anomaly (Fig. 4f). It is clear that this low-height anomaly contributes to the weakening of the subtropical high and westerlies are now extending from Indochina Peninsula, the SCS and all the way to the WNP, which marks the full onset.

The explained variance of the 850-hPa zonal winds anomalies by the 5–20-day mode during day −15 to day +15 shows that for the SCS domain and its neighborhood, the area of explained variance exceeding 80% can only be found over south China (Fig. 5), which suggests that the effect of acceleration of westerly winds by the approach of a mid-latitude front is limited to south China and northern SCS. This is consistent with the observation on the time-latitude plot of 850-hPa zonal wind (see Fig. 1a).

3.4 Collaboration between the 30–60-day and 5–20-day modes

The evolution of the 5–20-day mode 850-hPa height field is not unique during the onset period. In fact, the evolution of the height fields during day −6 to day −4 is remarkably similar to what has been presented in the previous section, with a low-height anomaly over WNP weakening the subtropical high (not shown). The 5–20-day mode alone therefore cannot explain the abrupt onset of the SCSSM. Some ‘collaboration’ with the 30–60-day mode must occur.

Although the 5–20-day mode appears to have a significant role in weakening the subtropical high (Fig. 4e), it is the meridional geopotential height gradient that determines the timing of the onset for the following reason. Suppose a mid-latitude trough and an MJO coexist over the south China and the equator respectively. Although the mid-latitude trough may lead to a weakening of the subtropical

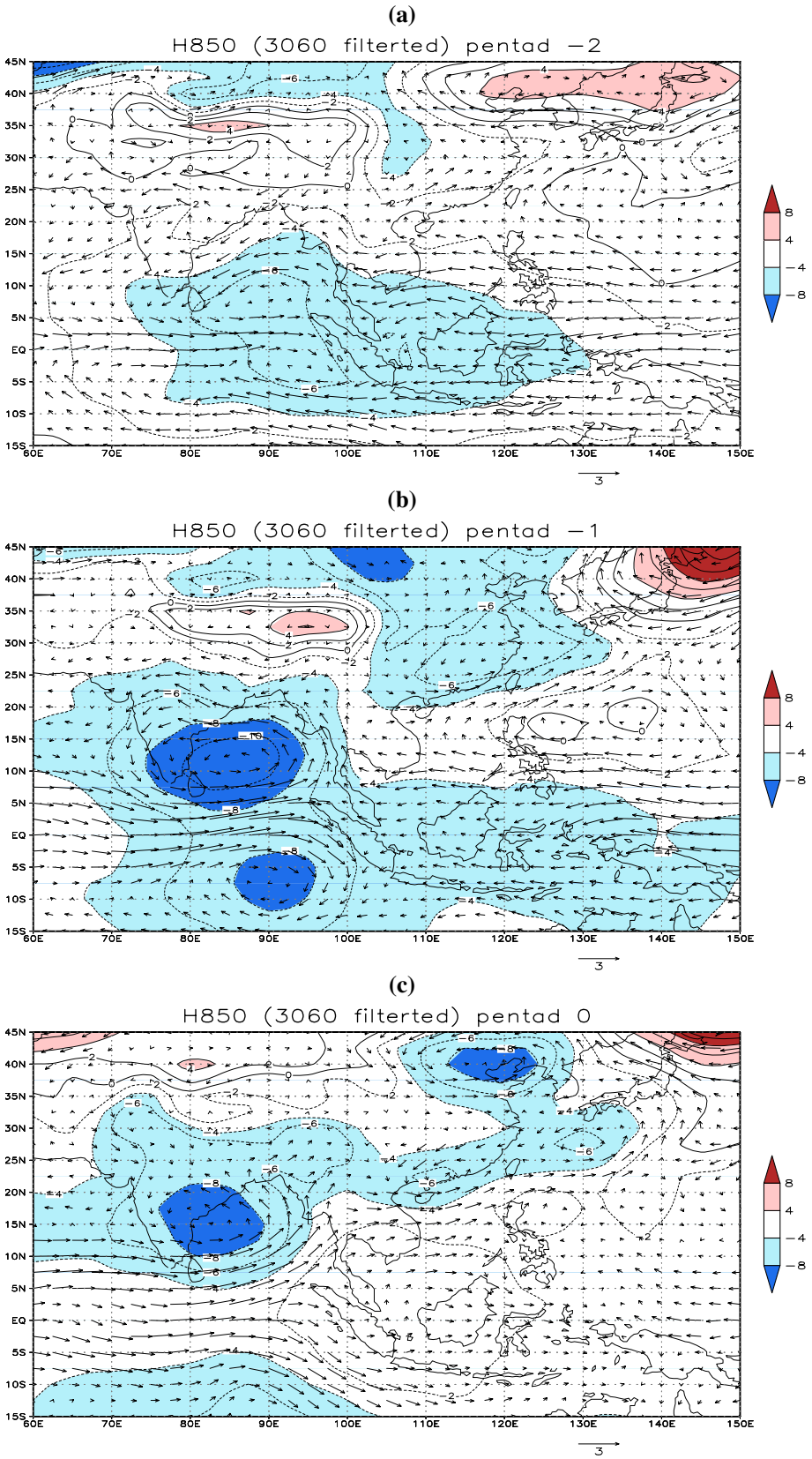

Fig. 2 A total of 30–60-day filtered composite 850-hPa geopotential height anomalies (m) and wind vectors (m s^{-1}) in **a** pentad −1, **b** pentad −2 and **c** pentad 0. Height anomalies ≤ (≥) −4 m (4 m) are *shaded* in *blue* (*red*)

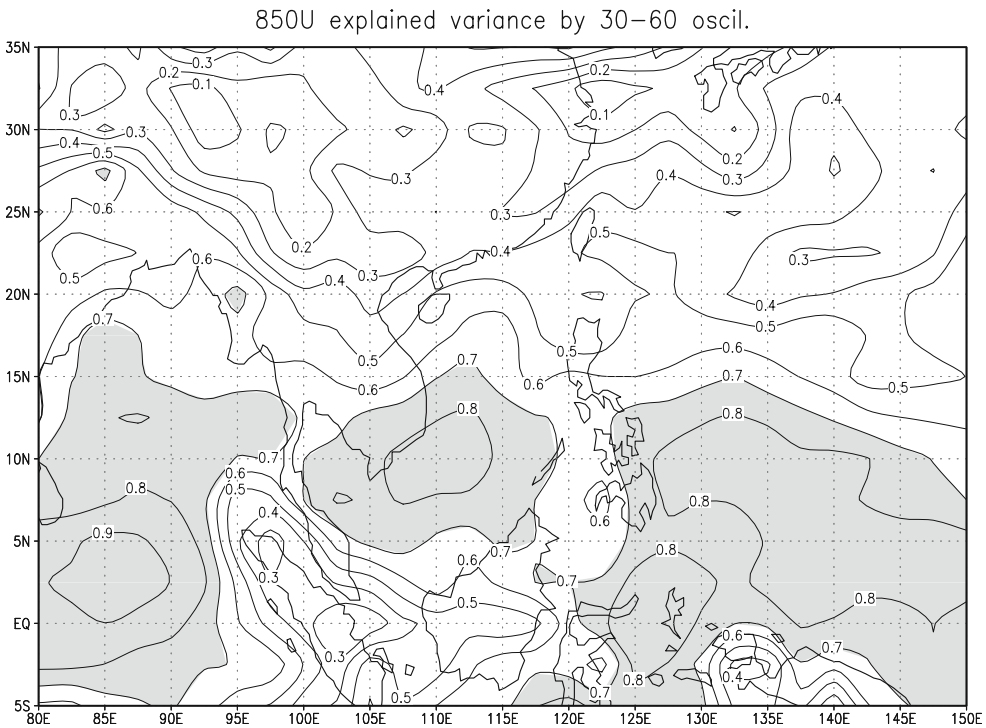

Fig. 3 Fractional variance of 850-hPa zonal wind explained by the 30–60-day mode for the period from day −15 to day +15. Areas with explained variance ≥0.7 are *shaded*

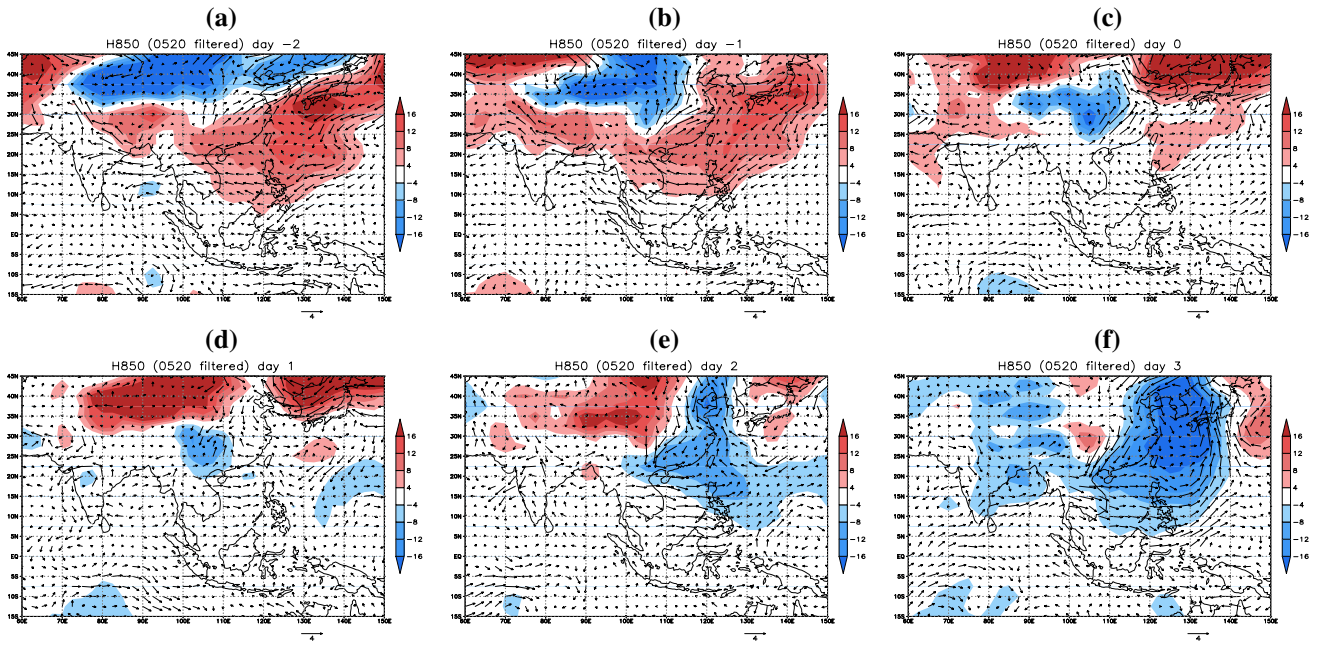

Fig. 4 A total of 5–20-day filtered composite 850-hPa geopotential height (gpm) and wind vectors (m s^{-1}) on **a** day −2, **b** day −1, **c** day 0, **d** day +1, **e** day +2, and **f** day +3. Height anomalies ≤(≥) 4 m are *shaded* in *blue* (*red*)

high, the meridional geopotential height gradient may still be negative due to the presence of the MJO at the equator so that westerly winds could not be induced over the SCS. The time series of the average 850-hPa zonal wind and the average 850-Pa meridional geopotential height gradient over the SCS domain (110–120°E, 5–20°N) are negatively correlated (Fig. 6a). In other words, easterly winds change to westerly winds when the meridional geopotential height gradient becomes negative. The meridional geopotential height gradient calculated from the 30–60-day mode is also comparable (Fig. 6b) although the variability of the 5–20-day mode is slightly higher. This means that although mid-latitude fronts may exist well before the onset and contributes to the weakening of the subtropical high, it is

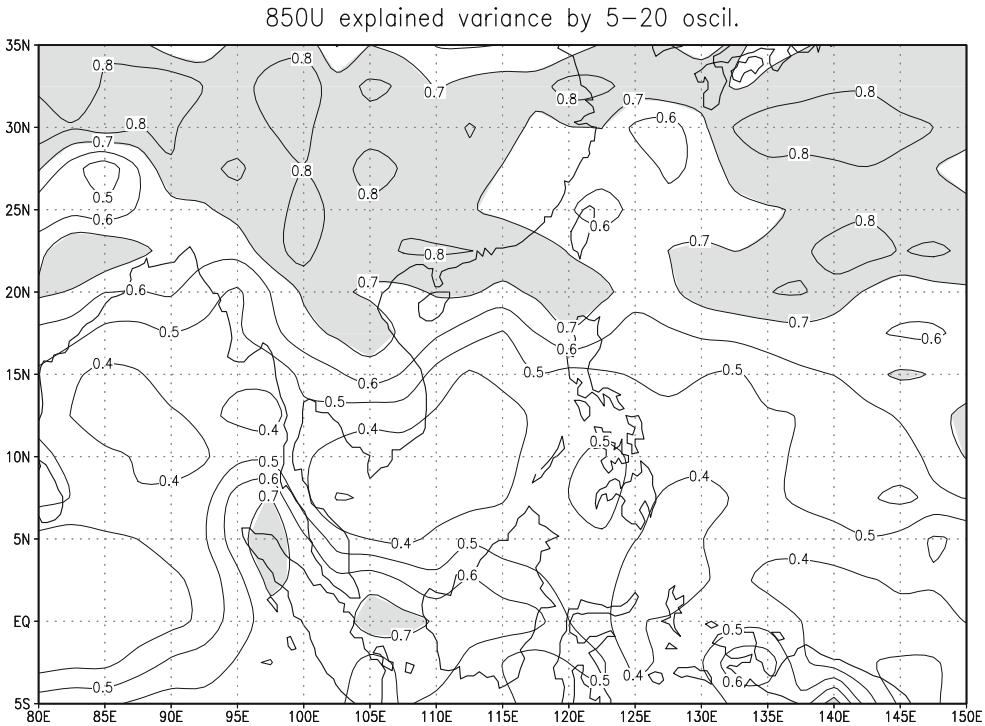

Fig. 5 Same as Fig. 3, but for the 5–20-day mode

not enough to counteract the meridional pressure gradient induced by the 30–60-day mode. In other words, the timing of the onset is determined by the 30–60-day mode rather than the 5–20-day mode.

4 Numerical experiments

4.1 Model description

In the previous section, we demonstrate how the 30–60-day mode could control the timing of the SCSSM onset. To further ascertain these findings, sensitivity experiments are carried out using the Regional Climate Model version 3 (hereafter RegCM3) developed at the International Centre for Theoretical Physics. The model has 18 vertical levels with the model top at 10 hPa, a 30-km horizontal resolution and a domain size of 265 × 165 grid points which approximately covers the region of 100–135°E 15°S–45°N. The initial atmospheric conditions and lateral boundary conditions are taken from the European Centre for Medium Range Weather Forecast ERA-40 reanalysis dataset. The sea surface temperature is taken from the NOAA Optimum Interpolation SST V2 weekly mean data with 1-degree latitude-longitude resolution. This weekly mean data are then linearly interpolated to daily values.

Physics of the model include the Kuo scheme (Anthes 1977) for convective precipitation; Pal scheme (Pal et al. 2000) for large-scale precipitation; BATS scheme (Dickinson et al. 1993) for surface processes; Holtslag scheme (Holtslag et al. 1990) for planetary boundary layer processes and NCAR CCM3 radiation scheme for radiation transfer (Kiehl et al. 1996).

All the experiments are initiated from 0000UTC on 1 April 1998 and integrated continuously through 30 June 1998. The year 1998 is chosen because studies have suggested that both the 30–60-day mode and mid-latitude fronts were essential for the SCSSM onset [for 30–60-day mode, see Straub et al. (2006); for mid-latitude fronts, see Chan et al. 2000]. The period of 1–14 April 1998 is considered as the spin-up period for the model and the results during this period will therefore not be analyzed.

4.2 Control experiment

The time-latitude cross-section of 850-hPa zonal wind from the control experiment, when compared with that of ERA-40, suggests that the SCSSM onset (around 20 May) is reasonably well simulated in terms of both the timing and intensity (cf. Fig. 7a, d). Cold air activities are also well simulated. Three cold air activities can be identified (marked by solid arrows in Fig. 7b), with the last one being particularly strong and penetrating deep into the south, which is very similar to the observations (Fig. 7e). Note also that the timing of the westerlies onset is coincident with the arrival of the cold front, which is again consistent with previous studies (Chan et al. 2000). Precipitation data for 1998 are taken from the Global Precipitation Climatology Project (GPCP). Precipitation is also reasonably well simulated over the SCS domain when compared to

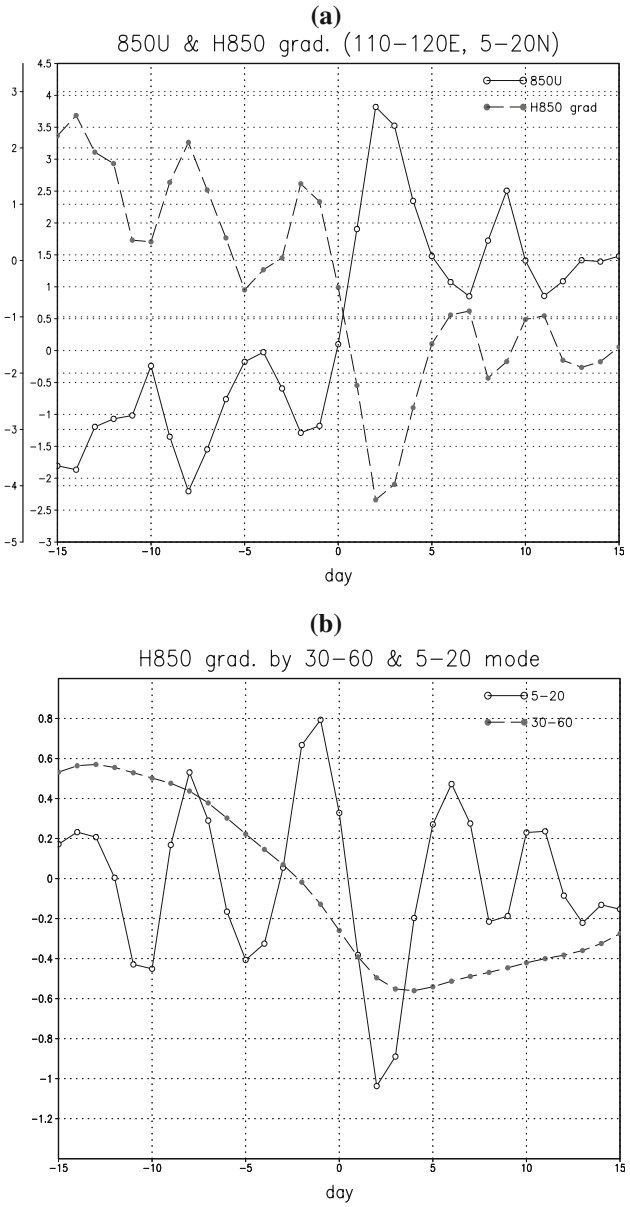

Fig 6 **a** Time series of composite 850-hPa zonal wind (*solid line*; units: m s^{-1}) and meridional geopotential height gradient (*dashed line*; unit: 1×10^{-5} gpm m^{-1}) averaged over the SCS (110–120°E, 5–20°N). Primary *y*-axis is for 850-hPa zonal wind and secondary *y*-axis is for the meridional geopotential height gradient. **b** 850-hPa meridional geopotential height gradient averaged over the SCS associated with the 30–60-day mode (*solid line*; unit: 1×10^{-5} gpm m^{-1}), and the 5–20-day mode (*dashed line*; unit: $1 \times 10^{-}$ gpm m^{-1})

GPCP (Fig. 7c, f). However, the model seems to underestimate the precipitation over the tropics. This may be due to the fact that Kuo scheme only produces rainfall when there is low-level moisture convergence. However, precipitation over the tropics is also related to static instability which the Kuo scheme does not account for. This underestimation of precipitation over the tropics also implies that the MJO, which is important for the onset, may be poorly represented in the model. In general, the model reproduces the SCSSM onset reasonably well apart from the deficiency in simulating tropical rainfall.

4.3 Experiment setup

Given the significance of the MJO found in the current composite results and previous studies (Straub et al. 2006), it is of interest to impose an artificial heat source/sink to investigate the impact the MJO could bring to the SCSSM onset. The stationary heat source/sink has the following from:

$$Q = \mathrm{CS}(p)\sin\left(2\pi\left(\frac{t - t_{\mathrm{initial}}}{\tau}\right)\right)\exp\left(-\left(\frac{\lambda - 115^{\circ}}{\delta\lambda}\right)^{2}\right) \times \exp\left(-\left(\frac{\phi}{\delta\phi}\right)^{2}\right) \quad (1)$$

where t_{initial} is the time where the heat source/sink emerges, λ and ϕ are longitude and latitude in degrees respectively, $\delta\lambda = 20^{\circ}$ and $\delta\phi = 10^{\circ}$. The centre of the heat source is set at 115°E and τ is the period of this standing oscillation, which is set to be 40 days, the approximate period of an MJO. The horizontal distribution is similar to the heating function used in Park et al. (1995) but with the eastward-moving component removed. The function $S(p)$ is the vertical distribution of the heat source/sink and has the form:

$$S(p) = \begin{cases} (p-20)(p-85)(p-90) & \text{for } 20 \le p \le 85 \\ 0 & \text{otherwise} \end{cases} \quad (2)$$

where p is the pressure and has the unit of kPa. This vertical distribution is similar to the one in Lau and Peng (1987). The heating peaks at 400 hPa with no heating above 200 hPa or below 850 hPa (Fig. 8). The parameter C is the amplitude of the heating which is chosen to give a heating rate of around 8°C day^{-1} at 400-hPa at the centre of the heating anomaly in the (EarlyMJO) experiment (see below). The sequences of the spatial distribution of this heat source/sink for (EarlyMJO) are shown in Fig. 9.

A total of four experiments are carried out (Table 2). The first three experiments aim at to study the effect of emergence time of the MJO on the SCSSM onset. Note that the heating source/sink is basically a sine function, and it takes 10 days to reach its peak. For example, for the (EarlyMJO) experiment, the heat source emerges on 20 Apr. The heating will peak on around 1 May which corresponds to an early MJO scenario. Similarly, for the (LateMJO) experiment, the heat source emerges on 10 May, and will reach its peak on 20 May which corresponds

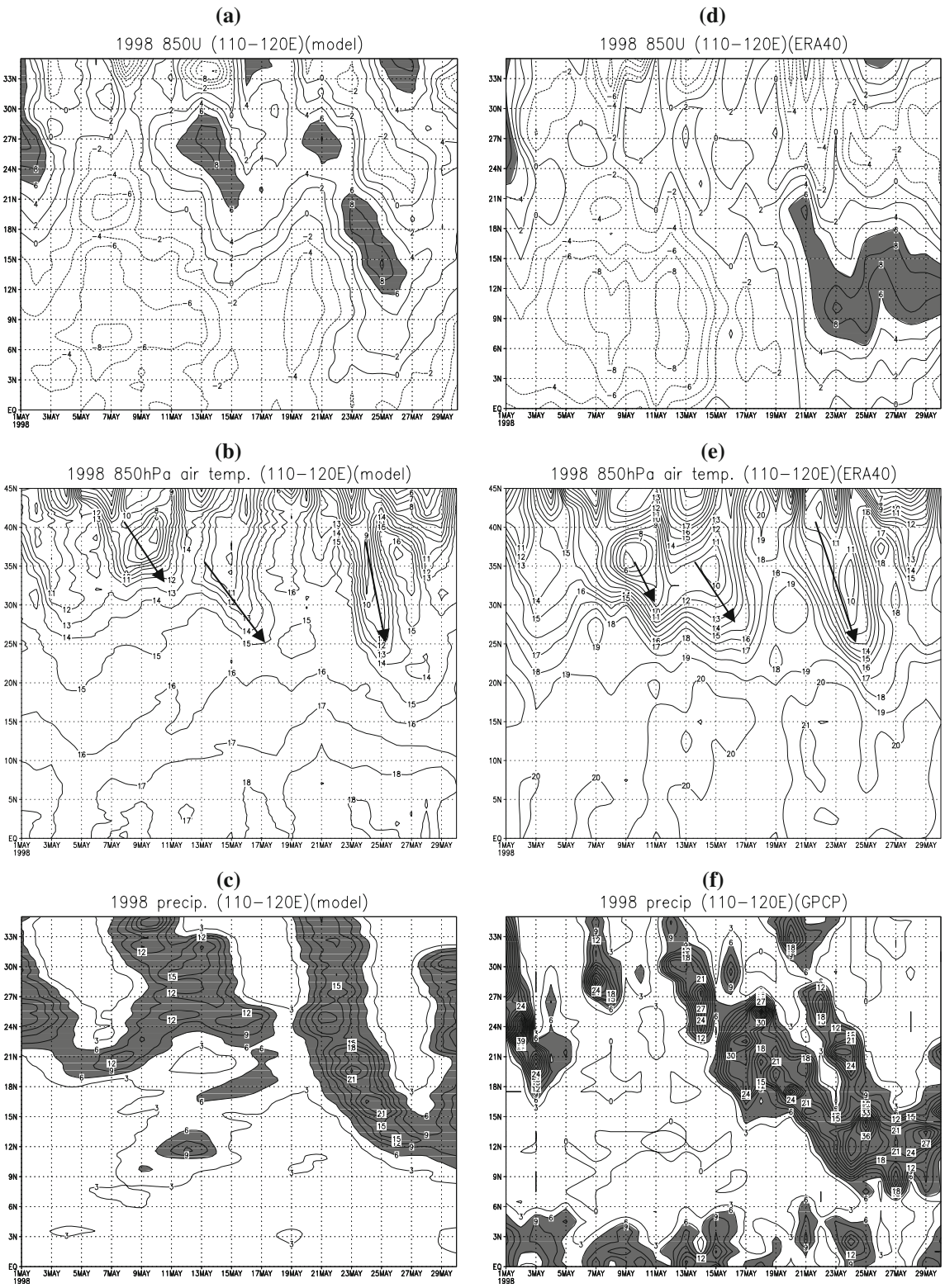

Fig. 7 Time-latitude cross-section of 1998 May (**a**) 850-hPa zonal wind (m s^{-1}; values $\geq$ 6 m s^{-1} are *shaded*). **b** 850-hPa air temperature (°C). **c** Precipitation rate (mm day^{-1}; values $\geq$ 6 mm day^{-1} are *shaded*) from the control experiment averaged over 110–120°E. **d** and **e** are the same as **a** and **b** respectively except that the data are from the ERA-40 dataset and **f** is the precipitation rate (mm day^{-1}) from the GPCP dataset

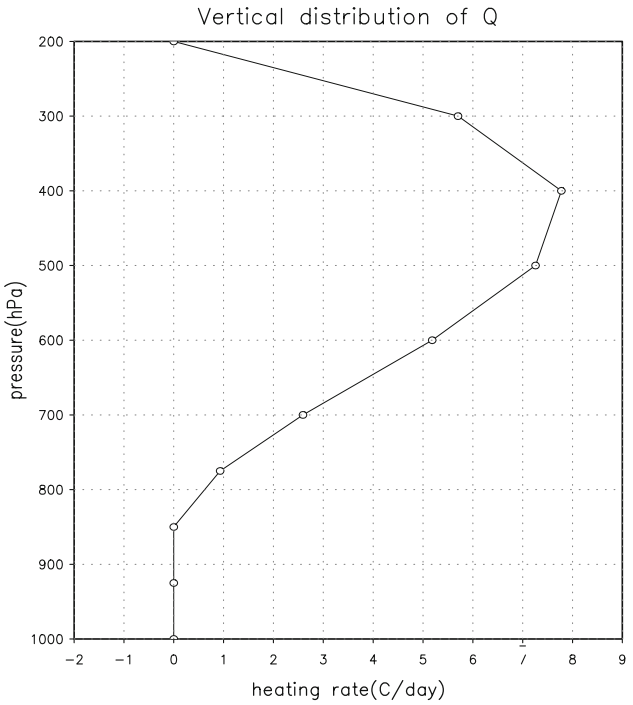

Fig. 8 Vertical distribution of heating rate at the centre of the heating anomalies for (EarlyMJO). Unit: °C day^{-1}

to a late MJO scenario. The last experiment aims at to study the effect of the strength of the MJO to the SCSSM onset. The maximum amplitude of the heating anomalies is increased to 10°C day^{-1} which corresponds to a strong and early MJO scenario.

5 Results

The time-latitude cross-section of 850-hPa zonal winds averaged over 110–120°E for the (EarlyMJO) experiment shows the onset of westerly winds occurring earlier on 15 May (Fig. 10) when compared to Fig. 8a because of the early emergence of the (artificial) heat source. The influence of the heat source/sink is depicted by taking the difference between the (EarlyMJO) and the control experiment. Initially, the low anomaly located at lower latitudes resulted in a positive meridional geopontential height gradient. Easterly winds are then induced over the SCS domain (Fig. 11a). A trough centered at 111°E, 12°N starts developing in pentad 3 of May (Fig. 11b). The centre of the trough is to the west of the heating centre at 115°E, which suggests that this trough is a Rossby wave response to the heating (Gill 1980). Strong westerlies and southwesterlies are found in its southern frank. By pentad 4, this trough has moved northward and covers the northern part of the SCS and east of Taiwan (Fig. 11c). Strong southwesterlies now move into the central SCS, which marks the early onset. It is interesting that this

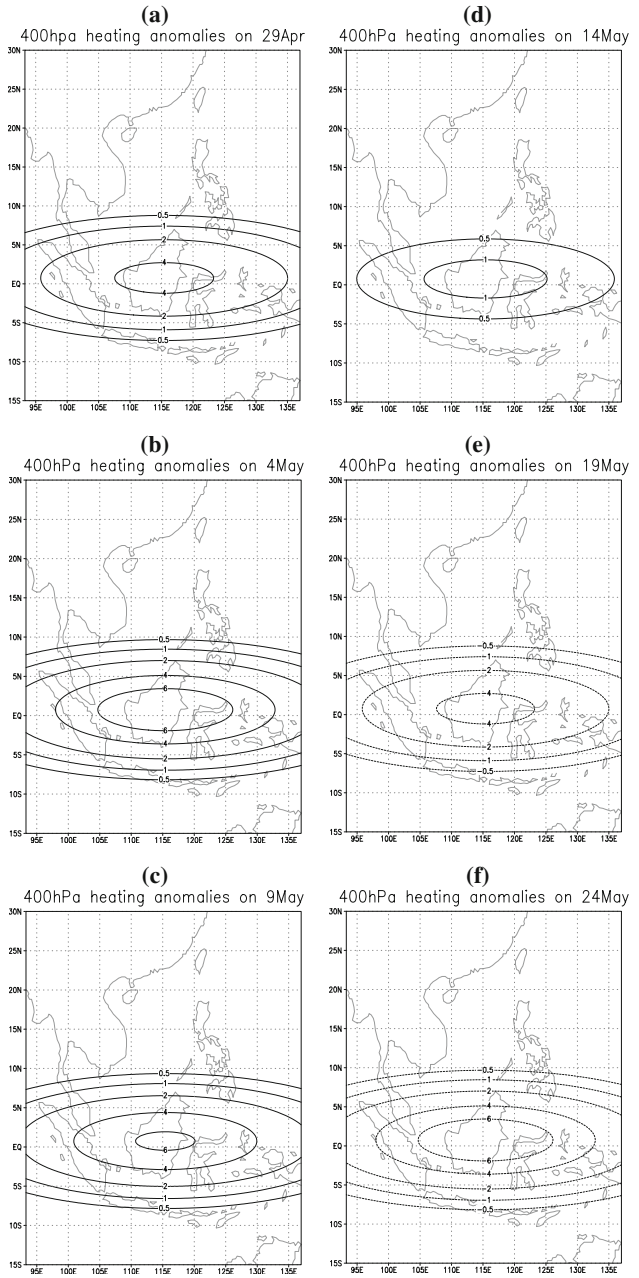

Fig. 9 Heating anomalies (unit: °C day^{-1}) at 400 hPa on **a** 29 Apr, **b** 4 May, **c** 9 May, **d** 14 May, **e** 19 May and **f** 24 May for (EarlyMJO)

northward-propagating trough is not found in the composite studies. Nonetheless, it is indeed a common feature in some years. For instance, Chen and Chen (1995) also found a northward-propagating trough in 1979 SCSSM onset which has some resemblance to this one (see their Fig. 10). The failure of the composite to capture this feature could be due to the fact that the position of this trough varies from year to year. For example, the northward-propagating trough in 1998 (observation, not model simulation, see Fig. 2 in Chan et al. 2002) is far more east than the one in 1979. Therefore,

Table 2 Parameters for the different experiments

See text for an explanation of the different experiments

	EarlyMJO	EarlyMJO2	LateMJO2	SEarlyMJO
$t_{initial}$	20 Apr	25 Apr	10 May	20 Apr
Max. heating rate at 400 hPa	8°C day^{-1}	8°C day^{-1}	8°C day^{-1}	10°C day

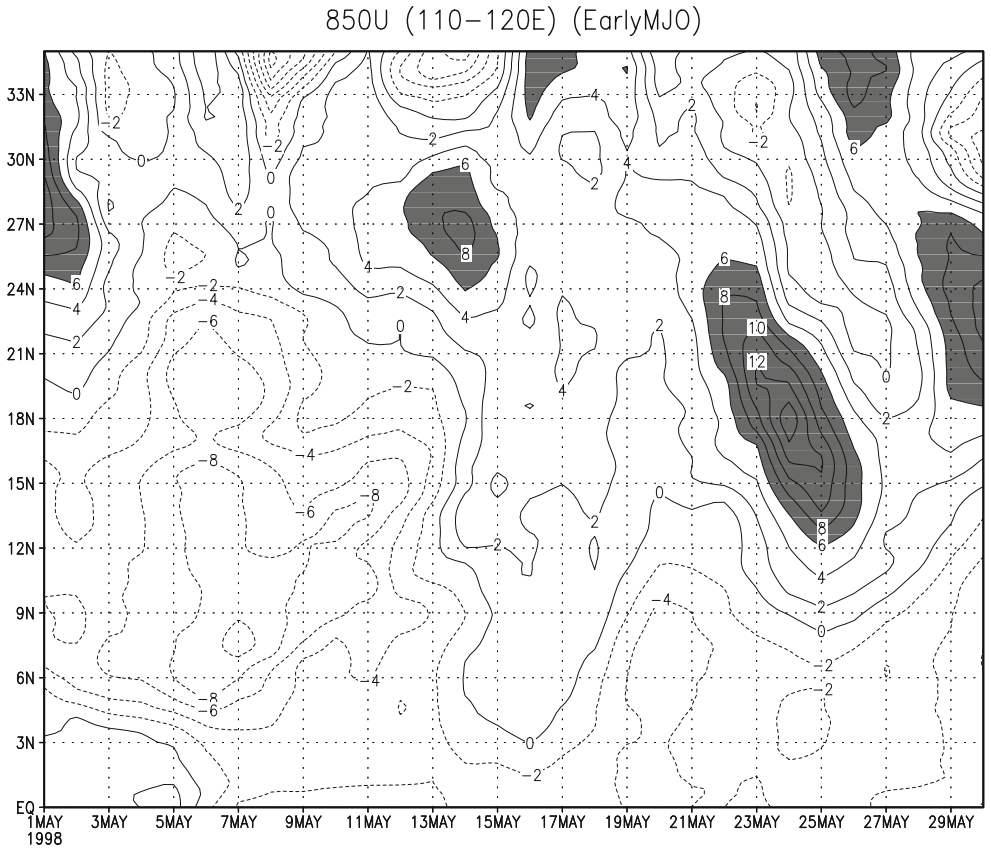

Fig. 10 Time-latitude cross-section of 850-hPa zonal wind (m s^{-1}) averaged over 110–120°E for the (EarlyMJO) experiment. Values $\geq$ 6 m s^{-1} are *shaded*

the northward-propagating feature may be smoothed out in the composite. Wang and Xie (1997) suggested that suppressed convection could lead to the disintegration of the Kelvin–Rossby wave packet and the emanation of Rossby waves over the WNP. The position of the northward-propagating trough may then be related to the position where equatorial convection is suppressed and this may in turn be related to the strength and extent of the MJO.

Despite the discrepancy between the model simulation and the composite studies, the basic mechanism is the same. When the heat source emerges over the Maritime continent, it imposes a positive meridional geopotential height gradient between the equator and the south China coast and hence, easterly winds are induced. When the trough moves northward, the meridional geopotential height gradient changes to negative, and westerly winds are induced. Note also that westerlies associated with the mid-latitude trough also strengthen on 25 May because of the background negative meridional geopotential height gradient induced by the heat source. However, due to the early emergence of the northward-moving trough induced by the heat source, the onset cannot be attributed to the mid-latitude front. (SEarlyMJO) further illustrates this mechanism. By increasing the amplitude of the heating anomaly to 10°C per day, the meridional geopontential gradient is further enhanced resulting an even stronger onset around 15 May (Fig. 12).

The emergence of the heat source in the (EarlyMJO2) experiment is 5 days later than that in the (EarlyMJO) experiment. As a result, it gives an impression that the northward-moving trough and MJO working together to induce the full onset on around 22 May (Fig. 13). Similar to

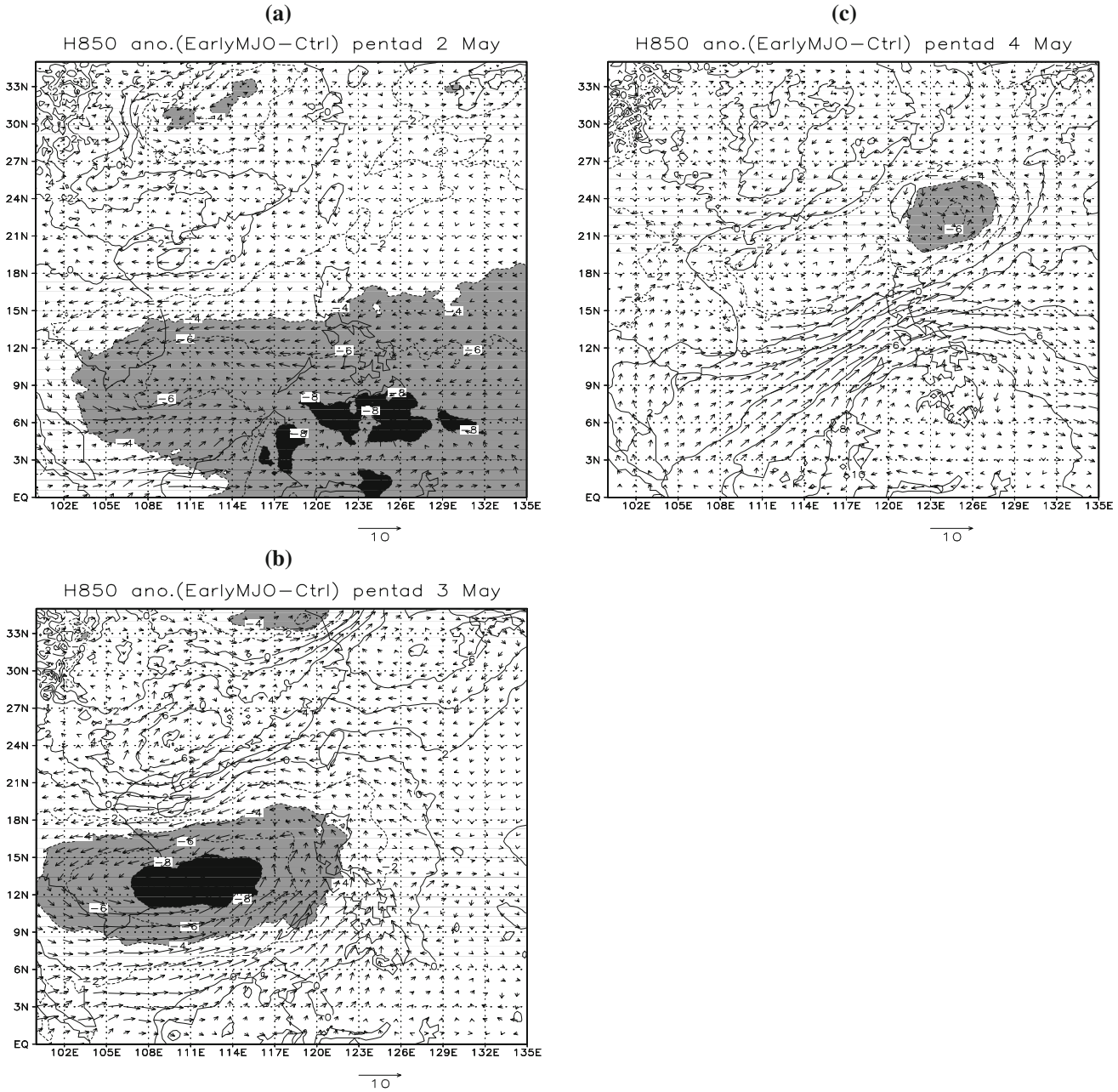

Fig. 11 A total of 850-hPa height and wind anomalies (with respect to the control experiment) in **a** pentad 2, **b** pentad 3 and **c** pentad 4 of May 1998 for the (EarlyMJO) experiment. Height anomalies ≤ -4 gpm (-8 gpm) are *light* (*dark*) *shaded*

the EarlyMJO case, the westerlies associated with the mid-latitude front strengthen due to the negative meridional geopotential gradient imposed by the heat source.

For the (LateMJO) experiment, the situation is a bit different. Although the timing of the onset for both the control and the (LateMJO) experiment is almost the same, it is evident that the westerlies associated with the mid-latitude trough are significantly reduced (Fig. 14a). This becomes even more obvious from the difference between the (LateMJO) and the control experiments (Fig. 14b). It is speculated that the coexistence of both a mid-latitude trough over the south China and a MJO at the equator greatly reduce the meridional geopotential height gradient over the SCS and hence the strength of westerly winds associated with the mid-latitude trough. The 1998 case is somewhat special because the synoptic forcing is very strong. For some other years in which the synoptic forcing is usually weaker, the onset would then possibly need to

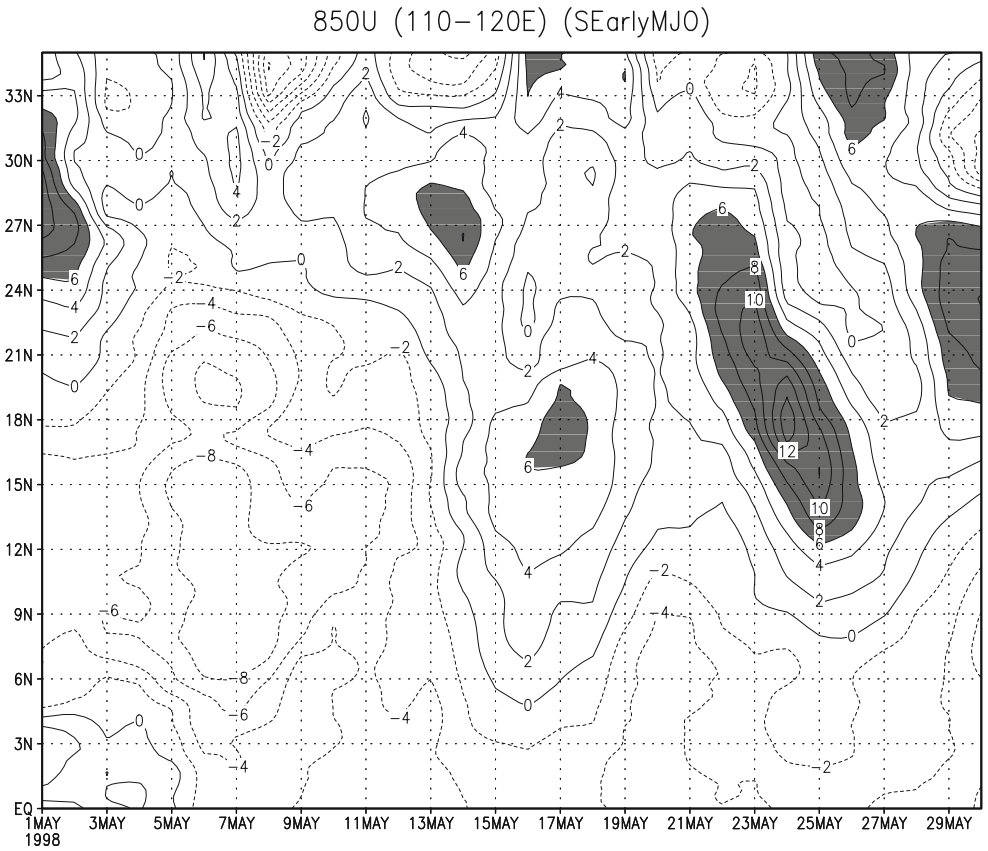

Fig. 12 Same as Fig. 10, but for the (SEarlyMJO) experiment

wait until the northward-moving trough move far enough north.

To summarize, the heat source controls the background meridional geopotential height gradient over the SCS. When it is in its active phase with low height anomaly at the equator, easterly winds are induced over the SCS. It is difficult for mid-latitude fronts to trigger the onset unless they are strong enough to counteract the meridional geopotential height gradient. After its peak phase when the equatorial convection has dissipated, the Rossby wave separates from the Kelvin-Rossby wave packet and moves northward. When the trough moves far enough north, the meridional geopotential height gradient changes its phase into negative and westerlies are induced over the SCS. The westerlies associated with the mid-latitude trough will strengthen and gives the impression that both the MJO and mid-latitude trough work together to induce the onset.

6 Conclusion and discussion

The study aims at to clarify the relative role of the MJO or Kelvin wave disturbances along the equator and synoptic-scale mid-latitude trough in inducing the SCSSM onset. A composite study of 9 years suggests that MJO and Kelvin waves play a major role in inducing the easterly-westerly shift over central SCS. The effect of acceleration of westerlies associated with a mid-latitude trough is limited to the northern part of the SCS. The numerical experiments show that the equatorial heat source associated with the MJO or Kelvin wave imposes a background meridional pressure gradient over the SCS. When the heating is at its peak at the equator, it imposes a positive meridional geopotential height gradient over the SCS and easterly winds are induced which in turn may significantly reduce the strength of the westerlies associated with the mid-latitude trough. After the heating at the equator has dissipated, a Rossby wave is induced and forms a northward-moving trough. When this trough gains enough latitude, the meridional geopotential height gradient reverses its sign and westerlies are induced. If no mid-latitude trough exists during this period, this northward-moving trough could alone induce the onset. If a mid-latitude trough exists, then it gives an impression that the northward-moving and the mid-latitude trough are in phase and work together to induce the onset.

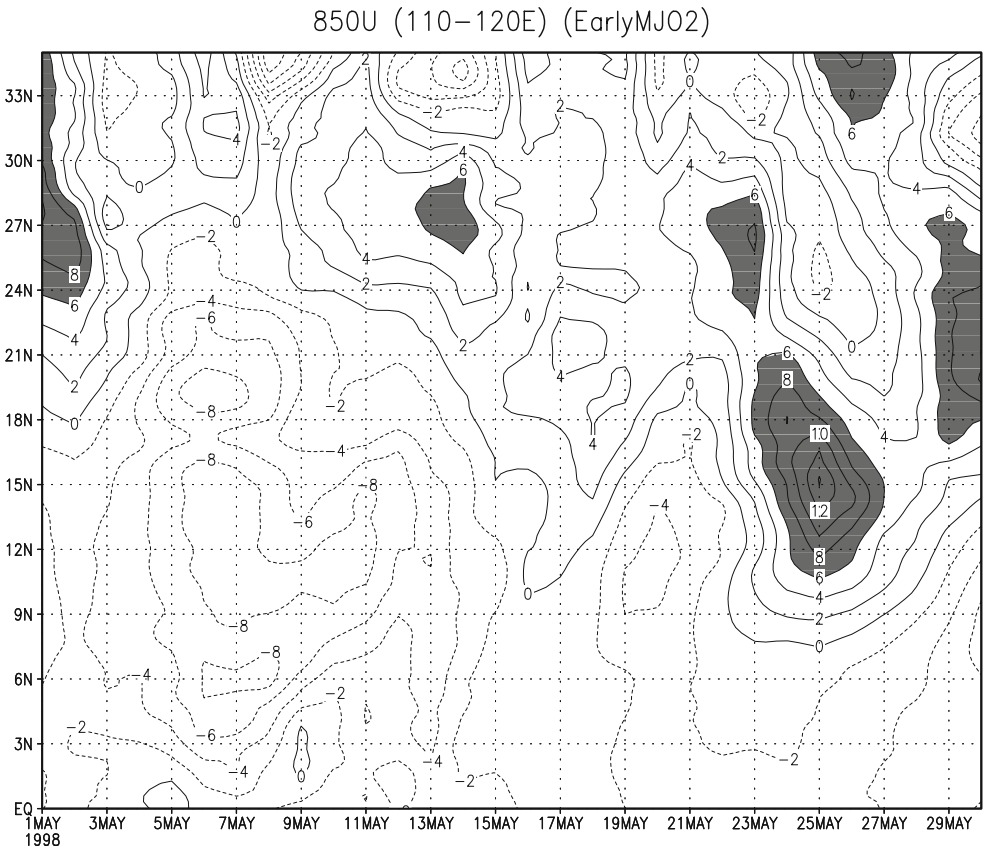

Fig. 13 Same as Fig. 10, but for the (EarlyMJO2) experiment

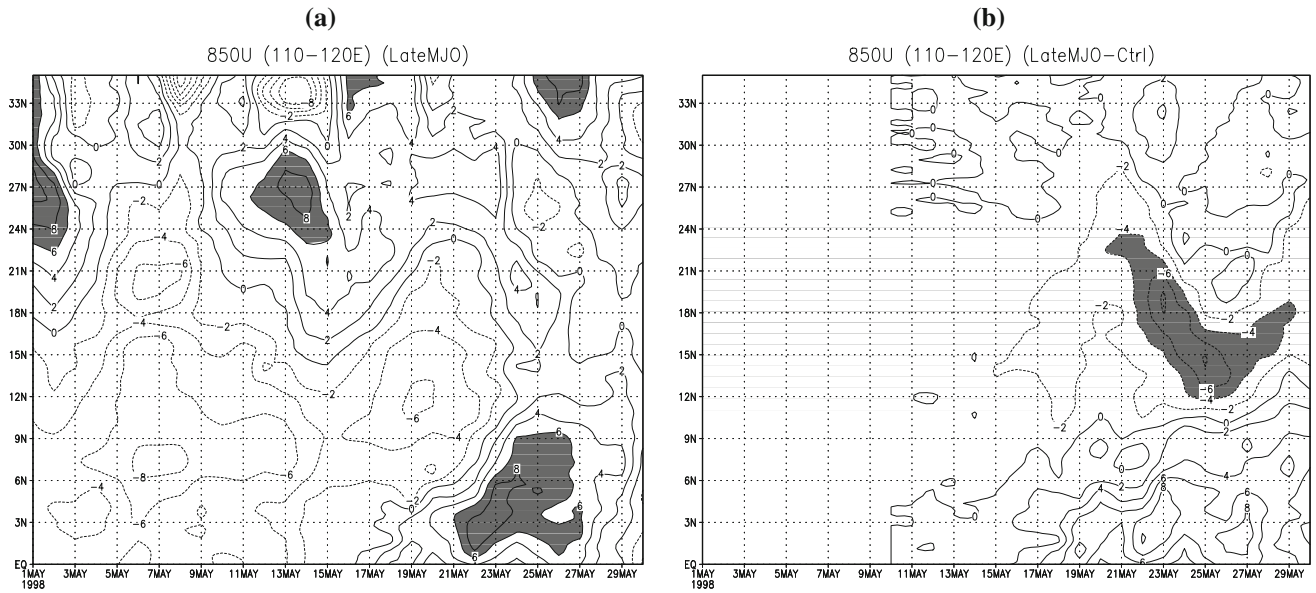

Fig. 14 **a** Same as Fig. 10 but for the (LateMJO) experiment. **b** A total of 850-hPa zonal wind differences between (LateMJO) and the control experiment (Differences ≤ -4 m s^{-1} are *shaded*)

6.1 Necessity of the eastward-moving component of MJO

While Straub et al. (2006) emphasizes that it is the MJO and Kelvin waves that are largely responsible for the easterly-westerly shift, the results of this study suggest that it is the large-scale meridional geopoential height gradient that controls the onset. Although both the current composite studies and Straub et al. (2006) have shown that the MJO or Kevin wave may be common during the onset period, it appears that an eastward-moving component of the MJO may not be necessary. The heat source/sink in the numerical experiments is stationary without any eastward-moving component and yet they produce a northward-moving trough that many studies observed and attributed to the eastward-moving MJO (Chen and Chen 1995; Chan et al. 2002). In fact, Wang and Rui (1990) observed independent northward-moving precipitation anomalies that exhibit no eastward movement of convection along the equator.

6.2 Causality of MJO and mid-latitude fronts

In the numerical experiments, the mid-latitude troughs are mainly forced by the boundary conditions although the strength of this mid-latitude trough could be influenced by the imposed heat source in situ. However, the composite studies suggest that there exists an equatorward movement of low height anomalies in the 30–60-day timescale which clearly has a mid-latitude origin (Fig. 2c). It is possible that this mid-latitude feature is physically linked to the MJO. For instance, Liu et al. (2002) suggested that the BOB onset vortex could excite an asymmetric Rossby wave, which could induce the intrusion of a mid-latitude trough. The numerical experiments did not examine this possible causality because the heat source/sink could only influence the dynamics and thermodynamics inside the model domain of the regional climate model but not the boundary conditions. It would be an interesting topic for future studies, and a global model is certainly needed to do so.

Acknowledgments The research of this study forms part of the Master of Philosophy research of the first author, which was supported by a Postgraduate Research Studentship from the City University of Hong Kong. Partial support was also provided by City University of Hong Kong Grant 7200098.

References

Anthes RA (1977) A cumulus parameterization scheme utilizing a one-dimensional cloud model. Mon Weather Rev 105:270–286

Chan JCL, Wang Y, Xu J (2000) Dynamic and thermodynamic characteristics associated with the onset of the 1998 South China Sea Summer Monsoon. J Meteor Soc Jpn 78:367–380

Chan JCL, Ai W, Xu J (2002) Mechanisms responsible for the maintenance of the 1998 South China Sea summer monsoon. J Meteor Soc Jpn 80:1103–1113

Chang CP, Chen GTJ (1995) Tropical circulations associated with southwest monsoon onset and westerly surges over the South China Sea. Mon Weather Rev 123:3254–3267

Chen TC, Chen JM (1995) An observational study of the South China Sea Monsoon during the 1979 summer: onset and life cycle. Mon Weather Rev 123:2295–2317

Dickinson RE, Henderson-Sellers A, Kennedy PJ (1993) Biosphere-atmosphere transfer scheme (BATS) version 1e as coupled to the NCAR community climate model. NCAR/TN-387+STR, p 72

Ding Y, Liu Y (2001) Onset and the evolution of the summer monsoon over the South China Sea during SCSSMEX field experiment in 1998. J Meteor Soc Jpn 79:255–276

Gill AE (1980) Some simple solutions for heat-induced tropical circulation. Q J R Meteor Soc 106:447–462

Hendon HH, Salby JL (1994) The life cycle of the Madden–Julian Oscillation. J Atmos Sci 51:2207–2219

Holtslag AAM et al (1990) A high-resolution airmass transformation model for short-range weather forecasting. Mon Weather Rev 118:1561–1575

Kiehl, JT, Hack J, Bonan G, Boville B, Briegleb B, Williamson D, Rasch P (1996) Description of the NCAR Community Climate Model (CCM3). NCAR Tech. Rep., TN-420+STR, p 152

Krishnamurti TN, Subrahmanyam D (1982) The 30–50-day mode at 850 mb during MONEX. J Atmos Sci 39:2088–2905

Lawrence DM, Webster PJ (2002) The boreal summer intraseasonal oscillation: Relationship between northward and eastward movement of convection. J Atmos Sci 59:1593–1606

Lau KM, Peng L (1987) Origin of low-frequency (intraseasonal) oscillation in the tropical atmosphere Part I: basic theory. J Atmos Sci 44:950–972

Liu YJ, Chan JCL, Mao J, Wu G (2002) The role of Bay of Bengal convection in the onset of the 1998 South China Sea summer monsoon. Mon Weather Rev 130:2731–2744

Madden RA (1986) Seasonal variation of the 40–50 day oscillation in the Tropics. J Atmos Sci 43:3138–3158

Madden RA, Julian PR (1971) Detection of a 40–50 day oscillation in the zonal wind in the tropical Pacific. J Atmos Sci 28:702–708

Madden RA, Julian PR (1972) Description of global-scale circulation cells in the tropics with a 40–50 day period. J Atmos Sci 29:1109–1123

Mao J, Chan JCL (2005) Intraseasonal variability of the South China Sea summer monsoon. J Clim 18:2388–2402

Pal JS, Small EE, Eltahir EAB (2000) Simulation of regional-scale water and energy budgets; representation of subgrid cloud and precipitation processes within RegCM. J Geophys Res 105:29579–29594

Park CK, Suarez MJ, Schubert SD (1995) Response of the zonally asymmetric flow to time-dependent tropical heating. J Atmos Sci 52:3738–3756

Straub KH, Kiladis GN, Ciesielski PE (2006) The role of equatorial waves in the onset of the South China Sea summer monsoon and the demise of El Nino during 1998. Dyn Atmos Ocean 42:216–238

Tao S, Chen L (1987) A review of recent research on the East Asian summer monsoon in China. In: Chang CP, Krishnamurti TN (eds) Monsoon meteorology. Oxford University Press, NY, pp 60–92

Wang B, Rui H (1990) Synoptic climatology of transient tropical intraseasonal convection anomalies: 1975–1985. Meteor Atmos Phys 44:43–61

Wang B, Xie X (1997) A model for the boreal summer intraseasonal oscillation. J Atmos Sci 54:72–86

Wang B, Xu X (1997) Northern hemisphere summer monsoon singularities and climatological intraseasonal oscillation. J Clim 10:1071–1085